Research Square

Preprints are preliminary reports that have not undergone peer review.
They should not be considered conclusive, used to inform clinical practice,
or referenced by the media as validated information.

Solving the Exact Solutions of the Fifth-order Dispersive Caudrey-Dodd-Gibbon Equation Based on the Feature-enhanced Direct Symbolic Computation Neural Network Algorithm

Jiang-Long Shen
Yibin University
Xia Li
xiali@yibinu.edu.cn

Yibin University

Research Article

Keywords: Fifth-order dispersion nonlinear wave equation, Feature enhancement, Direct symbolic computation, Neural networks

Posted Date: April 20th, 2026

DOI: https://doi.org/10.21203/rs.3.rs-9350197/v1

License: This work is licensed under a Creative Commons Attribution 4.0 International License.
Read Full License

Additional Declarations: No competing interests reported.

Version of Record: A version of this preprint was published at Nonlinear Dynamics on June 11th, 2026. See the published version at https://doi.org/10.1007/s11071-026-12729-9.

Noname manuscript No.
(will be inserted by the editor)

Solving the Exact Solutions of the Fifth-order Dispersive Caudrey-Dodd-Gibbon Equation Based on the Feature-enhanced Direct Symbolic Computation Neural Network Algorithm

Jiang-Long Shen · Xia Li

Received: date / Accepted: date

Abstract The Caudrey-Dodd-Gibbon (CDG) equation, a core constituent of the fifth-order Korteweg-de Vries (KdV)-type nonlinear wave equations, possesses exact solutions that are of pivotal significance for elucidating the mechanisms of wave propagation under the coupling effect of strong dispersion and intense nonlinearity. To mitigate the limitations inherent in traditional analytical methods for solving such high-order equations—encompassing narrow applicability, high computational complexity, and expression explosion a Feature-Enhanced Direct Symbolic Computation Neural Network(FEDSCNN) algorithm is proposed. This algorithm integrates the adaptive feature extraction capability of neural networks, the rigor of symbolic computation, and the advantages of feature enhancement. It constructs single-hidden-layer "2-5-3-1" and double-hidden-layer "2-5-2-2-1" architectures, and obtains exact solutions through a sequence of steps, namely symbolic derivation, equation mapping transformation, and constraint system solving. Experimental results validate that the proposed algorithm successfully acquires multiple categories of solitary wave solutions and periodic solutions for the CDG equation, with a zero error margin corroborated by the Maple symbolic computation engine. Furthermore, this algorithm circumvents the necessity of presetting solution forms, attains a higher convergence rate, and exhibits enhanced capability in capturing high-order terms. The present study not only furnishes an efficient and innovative approach for solving the CDG equation but also provides a general framework for the analytical solution of analogous high-order nonlinear wave equations, thereby facilitating the interdisciplinary integration of neural networks and symbolic computation.

Keywords Fifth-order dispersion nonlinear wave equation · Feature enhancement · Direct symbolic computation · Neural networks

J.L.Shen
School of Mathematics and Physics,
Yibin University, college street,Yibin, Sichuan 644000, China
E-mail: jlshen@yibinu.edu.cn(J.L.Shen)

X.Li (✉)
School of Mathematics and Physics,
Yibin University, college street,Yibin, Sichuan 644000, China
E-mail: xiali@yibinu.edu.cn(X.Li)

1 Introduction

The nonlinear wave equation, a fundamental mathematical tool for characterizing complex nonlinear phenomena in nature, holds profound significance across diverse disciplines such as fluid dynamics, plasma physics, and nonlinear optics. Ablowitz and Clarkson systematically established the analytical framework that bridges soliton theory and nonlinear evolution equations , thereby laying the theoretical foundation for research in this domain. Sulem et al. demonstrated the practical implications of nonlinear wave equations in the field of optics via their investigative work on the nonlinear optical properties of phase-modulated pulses[1,2]. The pursuit of exact solutions to these equations not only constitutes a core challenge in the field of mathematical physics but also provides direct theoretical support for elucidating the intrinsic dynamical mechanisms of nonlinear systems—including wave propagation, interaction, and stability. Wazwaz emphasized the pivotal role of exact solutions in elucidating physical phenomena from a methodological perspective[3].The fifth-order dispersion nonlinear wave CDG equation, in its standard form, is presented as:

$$u_t + u_{xxxxx} + 30uu_{xxx} + 30u_xu_{xx} + 180u^2u_x = 0, \quad (1)$$

It stands out as a prominent member of the fifth-order KdV-type equation family, falling into the same category of nonlinear evolution equations with profound physical implications as the Sawada-Kotera equation and the Kaup-Kupershmidt equation[4]. First proposed by Caudrey et al. in the course of their investigation into the hierarchical structure of fifth-order KdV-type equations, this equation incorporates fifth-order spatial derivatives and multiple nonlinear coupling terms. It precisely characterizes wave behaviors under the combined effects of strong dispersion and intense nonlinearity, and has been widely applied to physical contexts such as the propagation of shallow-water waves in fluids and the evolution of plasma acoustic waves [5]. Rani proposed three improved extension methods to systematically construct diverse soliton solutions for the CDG equation. The effectiveness and universality of these methods were verified, and their practical value was demonstrated through physical scenarios [6]. Meanwhile, Qin et al.'s study of the seventh-order CDG-KP equation in its high-dimensional extended form further emphasized the distinctive value of such high-order equations in depicting complex physical phenomena [7]. Thus, obtaining exact solutions to the CDG equation is of great theoretical and practical significance for enhancing our understanding of nonlinear wave behavior governed by fifth-order dispersion effects. For a long time, scholars have developed various traditional methods to obtain exact solutions of nonlinear wave equations. The inverse scattering transform method, proposed by Zakharov and Shabat, initiated the study of exact solutions for integrable systems and successfully solved classical models such as the KdV equation [8]. Hirota's bilinear method simplifies nonlinear terms through variable transformations and has been widely applied in constructing soliton solutions [9]. Wu's variational approach focuses on soliton solutions of nonlinear wave equations. By constructing fractal variational principles (based on the semi-inverse method), such solutions can be derived, proving to be an effective tool for solving low-order nonlinear equations [10]. Furthermore, the Lie group symmetry method, systematically expounded by Olver, transforms higher-order equations into lower-dimensional systems through symmetry reduction, showing advantages in constructing solutions for equations like the CDG equation [11]. Rafique derived exact solutions for the Sawada-Kotera and CDG equations, which are fifth order KdV type equations, through a unified algebraic framework. These solutions included solitons, periodic solutions, and Jacobi elliptic function solutions [12]. However, when applied to high-order equations, such as the CDG equation traditional methods encounter considerable limitations. The inverse scattering transform depends on the strict integrability of the equation, which limits its applicability. The bilinearisation process in the Hirota method is cumbersome for dealing with higher-order terms. Symbolic computation often suffers from "expression bloat," leading to inefficient calculations. The work of Koepf et al. combines theoretical depth with teaching utility, providing downloadable mathematical software codes [13, 14]. Arif F et al. systematically investigated analytical solutions for nonlinear convection - diffusion wave equations and successfully derived exact solutions, travelling wave solutions, and periodic solutions by comprehensively applying classical and modern analytical methods, including Lie symmetry analysis, the tanh method, and the Jacobi elliptic function approach [15].

The convergence of artificial intelligence and computational mathematics has led to groundbreaking approaches for solving nonlinear wave equations through the integration of neural networks and symbolic computation. Raissi et al. pioneered the Physical Information Neural Network (PINN), which embeds the control law of partial differential equations as symbolic constraints in neural network training. This unifies the solution of direct and inverse problems, establishing a new paradigm for approximating solutions to complex equations such as the Courier-Duhamel-Gaubert equation [16]. The Deep Galiokin Method(DGM), proposed by Sirignano et al., significantly improves the accuracy of solving higher-order equations. It approximates weak-form solutions via neural networks while using symbolic computation to handle integral constraints [17]. Zhu et al.'s Operator Information Regularisation method further strengthens network constraints through symbolic operator information, effectively enhancing the generalisation ability of neural networks [18]. Regarding feature enhancement mechanisms, Yang and Meng's feature - enhanced neural networks significantly improved the capture of key features in nonlinear equations by designing targeted feature extraction modules [19].

Zhang et al. recently developed neural network symbolic computation techniques, including bilinear neural networks and direct symbolic computation neural networks, have successfully constructed exact solutions for multiple nonlinear PDEs, validating the feasibility of this approach [20]. Luo et al., focusing on AI for Science applications, systematically reviewed the cutting - edge developments, core methodologies, application scenarios, and future directions of Physics - Informed Neural Networks (PINNs) in solving PDEs [20, 21]. Luo et al. focusing on the AI for Science context, systematically reviewed the cutting - edge progress, core methods, ap-

plication scenarios, and future directions of Physics - Informed Neural Networks (PINNs) in solving partial differential equations (PDEs)[21]. Dong and Li proposed a local extreme learning machine combined with domain decomposition methods, providing an engineering approach for the efficient solution of nonlinear PDEs [22]. Tang et al. addressed the issues of insufficient high - dimensional fitting accuracy and slow convergence in traditional PINNs for solving nonlinear PDEs by proposing a "PINNs + polynomial interpolation" fusion framework, offering a new efficient solution for complex nonlinear PDEs [23].

This technical approach has been extended to the broader realm of partial differential equations. Li et al. proposed an enhanced PINNs framework with "adaptive activation + fractional gradient enhancement" to tackle the non - locality and memory effects of fractional operators. This framework integrates physical constraints by means of symbolic derivation of Caputo-Fabrizio fractional derivatives and enhances the network's capability to fit fractional terms [24]. Chen et al. extended the core logic of "PINNs addressing direct and inverse problems for KdV-type equations" to fifth-order KdV-type equations, encompassing the CDG equation and the Sawada-Kotera equation.The direct problem focused on fitting the coupling between fifth - order dispersion terms and strong nonlinearities, while the inverse problem covered "coefficient identification + fractional order identification" [25]. Zeng et al. applied PINNs to the heat conduction equation with variable coefficients, enhancing the solution's reliability under complex boundary conditions by embedding physical constraints [26]. Zhang et al. focused on the core limitations of PINNs in solving PDEs, explored the root causes of failure, and proposed targeted future development directions [27].

Despite significant achievements in the analytical solution of the CDG equation, the Khater II method and variational iteration technique have successfully constructed its analytical solutions [28], and bilinear approaches have revealed the propagation characteristics of soliton molecules and hybrid solutions [29]. Moreover, the construction principles of periodic soliton solutions and lump wave solutions from analogous (3 + 1)-dimensional equations offer valuable insights for CDG equation research [30]. Simultaneously, neural network approaches show great potential. Shen et al.'s neural network symbolic computation algorithm has been adapted to solve high - dimensional nonlinear equations [31], and Wu Xuesha et al.'s bilinear residual network method has verified the feasibility of neural networks in handling variable - coefficient nonlinear PDEs [32]. Additionally, simulations of optical solitons in the generalised Kundu–Eckhaus equation and nonlinear Schrödinger equation have highlighted the advantages of intelligent algorithms in studying wave phenomena [33,34,35]. However, existing approaches are still restricted. Traditional analytical methods have limitations in solution form, and current neural networks often encounter issues such as insufficient feature representation and physical inconsistencies when dealing with the fifth - order dispersion term coupled with strong nonlinearity in the CDG equation.

To address these issues, this paper proposes the Feature - Enhanced Direct Neural Network (FEDSCNN) method. By using polynomial feature enhancement to strengthen the interaction between higher - order and nonlinear terms and embedding physical constraints to ensure solution reliability, it directly and efficiently constructs exact solutions to the CDG equation without relying on discrete or symbolic transformations. This methodology offers a novel perspective for the intelligent solution of higher-order nonlinear wave equations. This study systematically explores the application of the FEDSCNN algorithm in acquiring exact solutions to the CDG equation. Specific tasks encompass constructing a neural network architecture integrated with a fifth-order derivative feature extractor, designing a composite loss function composed of symbolic equation residuals and boundary conditions, and realizing precise gradient propagation via the Maple symbolic computation tool. Under diverse parameter configurations, typical solutions to the CDG equation—such as soliton and periodic solutions are obtained. This research not only offers an efficient new method for constructing exact solutions to the CDG equation but also holds promise for establishing a general framework for solving a class of high - order dispersive nonlinear wave equations. It further promotes the deep integration of neural networks and symbolic computation in the field of mathematical physics.

2 FEDSCNN algorithm

The FEDSCNN algorithm is illustrated in Figure 1. Initially, the expression of the construction function f of the FEDSCNN model is formulated. Subsequently, this expression f is substituted into the bilinear equation, yielding a complex algebraic polynomial. By gathering the coefficients of x,y and other relevant variables, an algebraic equation system with respect to the weights w and biases b is obtained. Finally, solving this algebraic equation system yields the coefficient solutions, which are subsequently substituted into the bilinear transformation u to derive the exact analytical solutions of the nonlinear partial differential equation. The tensor network model is illustrated in Figure 1.

$$
\begin{aligned}
&f = \omega_{l_n,\psi}\Phi_{l_n}(\xi_{l_n}),\\
&\xi_{l_i} = \omega_{l_{i-1},l_i}\Phi_{l_{i-1}}(\xi_{l_{i-1}}) + b_{l_i}, \quad i = 1, 2, \ldots, n
\end{aligned} \tag{2}
$$

In equation (2), $\omega_{i,j}$, i to j denotes the weight coefficient of neurons, and Φ is the activation function. If the terminal hidden layer satisfies the specified condition $\Phi_{l_n}(\xi) \geq 0$,it can be generalized to arbitrary functions. $l_n = \{m_{n-1}+1, m_{n-1}+2, \ldots, n\}$ represents the n-th layer space of the feature-enhanced symbolic computation neural network illustrated in Figure 1, where $l_0 = \{x_1, x_2, \ldots, x_n\}$, $l_1 = \{1, 2, \ldots, m_1\}$and $l_i = \{m_{i-1}+1, m_{i-1}+2, \ldots, m_i\}$ $(i = 2, 3, \ldots, n-1)$, j is a constant. The Core Procedures of the FEDSCNN algorithm for the CDG equation are as follows:

Step 1: Construct a feature-enhanced neural network architecture tailored to the CDG equation.

Input layer design: Feed in the independent variables x, t, and generate polynomial, exponential and trigonometric features via feature enhancement. These features capture the coupling behaviors between the fifth-order dispersive term and the nonlinear interaction term in the CDG equation. Specifically, polynomial features include quadratic, cubic and cross terms such as x^2, t^2, xt, x^3, t^3, while exponential and trigonometric features cover exponential decay, exponential growth and periodic terms such as $e^{kx}, e^{-kx}, \sin(kt), \cos(kt)$.

Hidden layer design: Employ a multi-layer architecture integrated with a composite activation function that combines hyperbolic tangent, high-order polynomial and exponential functions. The core objective is to enhance the fitting capability for the dispersive effects induced by the fifth-order derivative term and the strong nonlinear interaction term.

Output layer design: Output the probe function $u(x, t)$, and construct the analytical expression of the potential solution via the network weights and bias parameters.

Step 2: Symbolic derivation of full-order partial derivatives for the CDG equation.

The Maple symbolic computation engine is employed to expand the full-order partial derivatives of the output function $u(x, t)$, with a specific focus on computing the key derivative terms involved in the CDG equation: $u_t, u_x, u_{xx}, u_{xxx}, u_{xxxx}, u_{xxxxx}$ and u^2u_x. High-dimensional composite operations are recursively addressed via the chain rule to ensure the rigor of the derivation process for the fifth-order derivative term, thereby eliminating the cumulative effects of truncation errors from numerical differentiation on high-order terms.

Step 3: Symbolic mapping transformation of the CDG equation.

All orders of partial derivatives obtained in Step 2 are substituted into Equation (1), the fifth-order CDG equation. Algebraic operations including rationalization and combination of like terms are performed to eliminate redundant terms, and the equation is transformed into a simplified form that only contains u, all orders of its derivatives, network weights and biases. This process achieves dimension-reducing mapping from the fifth-order PDE constraint to an algebraic constraint.

Step 4: Construction of CDG-specific parameter constraint equations.

Grouping strategy: Fine grouping is performed on the transformed equation according to the powers of x and t, the order of exponential functions and the frequency of trigonometric functions, with a specific focus on the coefficient architectures of the fifth-order derivative term and the nonlinear interaction term.

Constraint generation: The coefficients of all grouped terms are set to zero to generate algebraic constraint equations for network parameters. The parameter space is compressed via normalization processing, prioritizing the parameter subspace that satisfies the dispersive and nonlinear balance conditions of the CDG equation.

Step 5: Closed-loop verification and extraction of CDG analytical solutions.

The screened parameters are substituted back into the probe function $f(x, t)$ to reconstruct the candidate analytical solution. This reconstructed solution is subsequently substituted into the CDG equation for symbolic validation, with particular emphasis on verifying the balance relationship between the fifth-order derivative term and the nonlinear interaction term. The accuracy of the acquired solutions is optimized via the adjustment of feature enhancement parameters, and analytical forms that strictly satisfy the CDG equation—encompassing soliton solutions and periodic solutions—are ultimately derived.

This process specifically captures the fifth-order dispersive properties of the CDG equation via feature enhancement, while integrating the rigor of symbolic computation to achieve precise mapping from the neural network's parameter space to the analytical solution space of the equation. The FEDSCNN algorithm possesses a distinct advantage in surmounting the limitations associated with traditional raw variable input: it expands the model's capability to capture nonlinear relationships, alleviates solution errors induced by inadequate feature representation, and thereby facilitates the establishment of accurate analytical solutions for nonlinear partial differential equations.

This model incorporates merely a single hidden layer. For example, a single-hidden-layer feature enhancement

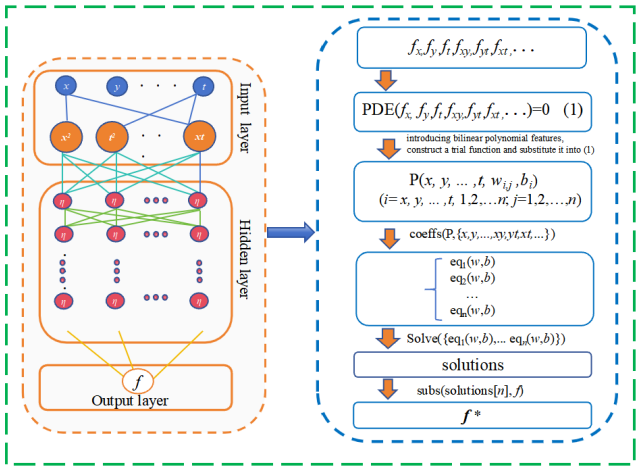


Fig. 1: FEDSCNN Model

network with three specific functions can cover the constructed probe functions, as illustrated in Figure 2, while a dual-hidden-layer feature enhancement network with four specific functions achieves the same coverage, as depicted in Figure 3.

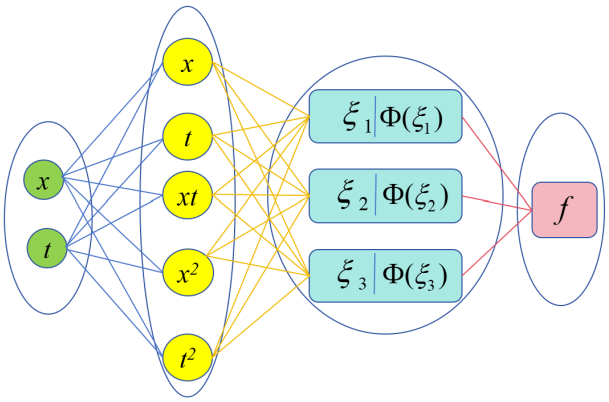


Fig. 2: Single-Hidden Layer Feature Enhancement '2-5-3-1' Neural Network Model

3 FEDSCNN Algorithm for Obtaining Exact Solutions to CDG Equations

By deploying the FEDSCNN algorithm for feature enhancement tasks in two distinct neural network architectures—specifically, the single-hidden-layer 2-5-3-1 model and the dual-hidden-layer 2-5-2-2-1 model—corresponding probe functions were selected to derive the exact solution of the CDG equation. Subsequently, three-dimensional plots, density plots, contour plots, and contour line plots of the acquired solution were generated to conduct an in-depth characterization of its fundamental properties.

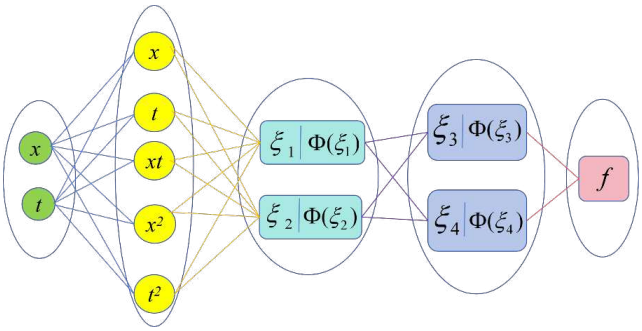


Fig. 3: Dual-Hidden-Layer Feature-Enhanced '2-5-2-2-1' Neural Network Model

3.1 Single-Hidden Layer Feature Enhancement '2-5-3-1' Neural Network Model

The mathematical expression corresponding to the single-hidden-layer feature-enhanced 2-5-3-1 neural network model illustrated in Figure 3.1 is selected as the test function.

$$
\begin{aligned}
\xi_1 &= w_{x,1}\cdot x + w_{t,1}\cdot t + w_{xt,1}\cdot xt \\
&\quad + w_{x^2,1}\cdot x^2 + w_{t^2,1}\cdot t^2 + b_1, \\
\xi_2 &= w_{x,2}\cdot x + w_{t,2}\cdot t + w_{xt,2}\cdot xt \\
&\quad + w_{x^2,2}\cdot x^2 + w_{t^2,2}\cdot t^2 + b_2, \\
\xi_3 &= w_{x,3}\cdot x + w_{t,3}\cdot t + w_{xt,3}\cdot xt \\
&\quad + w_{x^2,3}\cdot x^2 + w_{t^2,3}\cdot t^2 + b_3, \\
f &= w_{1,f}\cdot \sin(\xi_1) + w_{2,f}\cdot \cos(\xi_2) + w_{3,f}\cdot e^{\xi_3} + b_4,
\end{aligned}
\tag{3}
$$

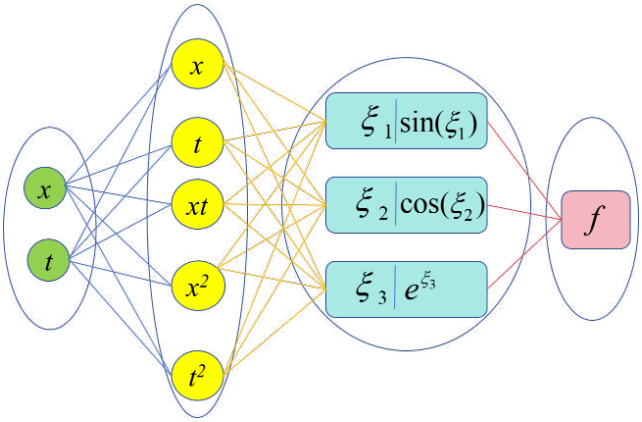


Fig. 4: Single-Hidden Layer Feature Enhancement '2-5-3-1' Neural Network Model

$$
\begin{aligned}
f = {} & w_{1,f} \sin\left(w_{x,1}x + w_{t,1}t + w_{xt,1}xt + w_{x^2,1}x^2 + w_{t^2,1}t^2 + b_1\right) \\
& + w_{2,f} \cos\left(w_{x,2}x + w_{t,2}t + w_{xt,2}xt + w_{x^2,2}x^2 + w_{t^2,2}t^2 + b_2\right) \\
& + w_{3,f} \exp\left(w_{x,3}x + w_{t,3}t + w_{xt,3}xt + w_{x^2,3}x^2 + w_{t^2,3}t^2 + b_3\right) + b_4,
\end{aligned} \tag{4}
$$

The activation functions are defined as $\Phi_1(\xi_1) = \sin(\xi_1)$, $\Phi_2(\xi_2) = \cos(\xi_2)$, and $\Phi_3(\xi_3) = e^{\xi_3}$.

As shown in Figure 4, with the activation functions set to $\Phi_1(\xi_1) = \xi_1^2$, $\Phi_2(\xi_2) = \xi_2^2$, and $\Phi_3(\xi_3) = e^{\xi_3}$, the probe function for the solution can be obtained as follows:

where b_i for $i = 1, 2, 3$, $w_{j,f}$ for $j = 1, 2$, and $w_{k,1}$ for $k = x, t, xt, x^2, t^2$ are real numbers.

Substituting the probe function (4) into the CDG equation (1) results in a complex algebraic equation. Terms are collected and the coefficient of each term is set to zero, which satisfies the CDG equation. This process yields a system of algebraic equations, whose solution yields the corresponding analytical results.

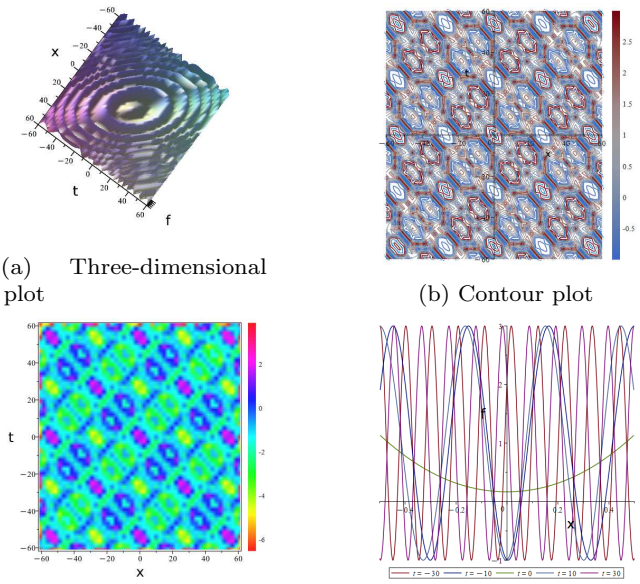
Case 1

$$
\begin{cases}
t = t,\ x = x,\ b_4 = b_4,\ w_{1,4} = 0,\ w_{2,4} = w_{2,4}, \\
w_{3,4} = 0,\ w_{t,1} = w_{t,1}, w_{t,2} = -2\hbar v_{t^2,2} - x w_{xt,2}, \\
w_{t,3} = w_{t,3},\ w_{x,1} = w_{x,1},\ w_{x,2} = -\hbar v_{xt,2} - 2x w_{x^2,2}, \\
w_{x,3} = w_{x,3},\ w_{xt,1} = w_{xt,1},\ w_{xt,2} = w_{xt,2}, \\
w_{xt,3} = w_{xt,3},\ w_{t^2,1} = w_{t^2,1}, w_{t^2,2} = w_{t^2,2}, \\
w_{t^2,3} = w_{t^2,3},\ w_{x^2,1} = w_{x^2,1},\ w_{x^2,2} = w_{x^2,2}, \\
w_{x^2,3} = w_{x^2,3}.
\end{cases} \tag{5}
$$

For Case 1, Equation (5) is substituted into Equation (4) and simplified, resulting in the analytical solution of the CDG equation presented in Equation (6):

$$
f = b_4 + w_{2,4} \cos\left(-t^2 w_{t^2,2} - t x w_{xt,2} - x^2 w_{x^2,2} + b_2\right) \tag{6}
$$

To verify the accuracy of Result (6), the analytical solution corresponding to this result is substituted into the left-hand side of Equation (1). By means of the Maple symbolic computation engine, symbolic simplification confirms that the left-hand side of Equation (1) is equal to zero, thus verifying the reliability, accuracy, and zero-error property of the analytical solution associated with Result (6). This further underscores a key advantage of the proposed method over classical neural network approaches—whereas the latter only yield approximate solutions, the bilinear feature-enhanced symbolic computation neural network algorithm is capable of deriving rigorous exact analytical solutions.



(a) Three-dimensional plot (b) Contour plot (c) Density plot (d) Curve chart

Fig. 5: Three-dimensional plot, density plot, contour plot and contour lines of the solution to Equation (6)

By setting $b_4 = 1$, $w_{2,4} = 2$, $w_{t^2,2} = 2$, $w_{xt,2} = 2$, $w_{x^2,2} = 2$, $b_2 = 2$, the visualization of the solution (Figure 5) is generated:

- Figure 5(a) shows the three-dimensional image for $t \in (-60, 60)$ and $x \in (-60, 60)$;
- Figure 5(b) presents the contour plot of the solution corresponding to Equation (6);
- Figure 5(c) displays the density plot;
- Figure 5(d) depicts the curve plot of u versus x over the domain $(-60, 60)$.

The mathematical expression corresponding to the single-hidden-layer feature-enhanced "2-5-3-1" neural network model illustrated in Figure 6 is chosen as the

probe function: (9)

$$\begin{aligned}
\xi_1 &= w_{x,1}\cdot x + w_{t,1}\cdot t + w_{xt,1}\cdot xt + w_{x^2,1}\cdot x^2 \\
&\quad + w_{t^2,1}\cdot t^2 + b_1, \\
\xi_2 &= w_{x,2}\cdot x + w_{t,2}\cdot t + w_{xt,2}\cdot xt + w_{x^2,2}\cdot x^2 \\
&\quad + w_{t^2,2}\cdot t^2 + b_2, \\
\xi_3 &= w_{x,3}\cdot x + w_{t,3}\cdot t + w_{xt,3}\cdot xt + w_{x^2,3}\cdot x^2 \\
&\quad + w_{t^2,3}\cdot t^2 + b_3, \\
f &= w_{1,f}\cdot \sinh(\xi_1) + w_{2,f}\cdot \cosh(\xi_2) \\
&\quad + w_{3,f}\cdot e^{\xi_3} + b_4,
\end{aligned} \tag{7}$$

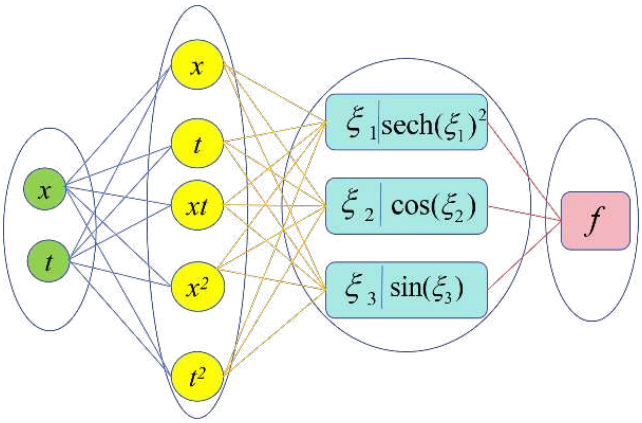


Fig. 6: Single-Hidden Layer Feature Enhancement '2-5-3-1' Neural Network Model

The activation functions are defined as $\Phi_1(\xi_1) = \sinh(\xi_1)$, $\Phi_2(\xi_2) = \cosh(\xi_2)$, and $\Phi_3(\xi_3) = e^{\xi_3}$.

As shown in Figure 6, with the activation functions set to $\Phi_1(\xi_1) = \sinh(\xi_1)$, $\Phi_2(\xi_2) = \cosh(\xi_2)$, and $\Phi_3(\xi_3) = e^{\xi_3}$, the probe function for the solution is obtained as follows:

where b_i for $i = 1, 2, 3$, $w_{j,f}$ for $j = 1, 2$, and $w_{k,1}$ for $k = x, t, xt, x^2, t^2$ are real numbers.

Equation (8) is substituted into the CDG equation (1), resulting in a complex algebraic equation. Terms are collected and the coefficient of each term is set to zero, which satisfies the CDG equation. This process yields a system of algebraic equations, whose solution yields the corresponding analytical solution.

Case 1

$$\begin{cases}
b_1 = b_1,\ t = t,\ x = x,\ b_4 = b_4,\ w_{1,4} = 0, w_{2,4} = w_{2,4}, \\
w_{3,4} = 0,\ w_{t,1} = w_{t,1}, w_{t,2} = -2tw_{t^2,2} - xw_{xt,2}, \\
w_{t,3} = w_{t,3}, w_{x,1} = w_{x,1}, w_{x,2} = -tw_{xt,2} - 2xw_{x^2,2}, \\
w_{x,3} = w_{x,3}, w_{xt,1} = w_{xt,1}, w_{xt,2} = w_{xt,2},\ w_{xt,3} = w_{xt,3}, \\
w_{t^2,1} = w_{t^2,1}, w_{t^2,2} = w_{t^2,2}, w_{t^2,3} = w_{t^2,3},\ w_{x^2,1} = w_{x^2,1}, \\
w_{x^2,2} = w_{x^2,2},\ w_{x^2,3} = w_{x^2,3}
\end{cases}$$

For Case 1, Equation (9) is substituted into Equation (8) and simplified, resulting in the analytical solution of the CDG equation presented in Equation (10):

$$f = b_4 + w_{2,4}\cosh\left(-t^2 w_{t^2,2} - txw_{xt,2} - x^2 w_{x^2,2} + b_2\right) \tag{10}$$

To verify the accuracy of Result (10), the analytical solution corresponding to this result is substituted into the left-hand side of Equation (1). By means of the Maple symbolic computation engine, symbolic simplification confirms that the left-hand side of Equation (1) is equal to zero, thereby validating the reliability, accuracy, and zero-error property of the analytical solution associated with Result (10).

By setting $b_4 = 1$, $w_{2,4} = 2$, $w_{t^2,2} = 2$, $w_{xt,2} = 2$, $w_{x^2,2} = 2$, $b_2 = 2$, the visualization of the solution (Figure 7) is generated:

- Figure 7(a) shows the three-dimensional image for $t \in (-30, 30)$ and $x \in (-30, 30)$;
- Figure 7(b) presents the contour plot of the solution corresponding to Equation (10);
- Figure 7(c) displays the density plot;
- Figure 7(d) depicts the curve plot of u versus x over the domain $(-150, 150)$.

The mathematical expression corresponding to the single-hidden-layer feature-enhanced "2-5-3-1" neural network model illustrated in Figure 8 is chosen as the probe function:

$$\begin{aligned}
\xi_1 &= w_{x,1}\cdot x + w_{t,1}\cdot t + w_{xt,1}\cdot xt \\
&\quad + w_{x^2,1}\cdot x^2 + w_{t^2,1}\cdot t^2 + b_1, \\
\xi_2 &= w_{x,2}\cdot x + w_{t,2}\cdot t + w_{xt,2}\cdot xt \\
&\quad + w_{x^2,2}\cdot x^2 + w_{t^2,2}\cdot t^2 + b_2, \\
\xi_3 &= w_{x,3}\cdot x + w_{t,3}\cdot t + w_{xt,3}\cdot xt \\
&\quad + w_{x^2,3}\cdot x^2 + w_{t^2,3}\cdot t^2 + b_3, \\
f &= w_{1,f}\cdot \operatorname{sech}^2(\xi_1) + w_{2,f}\cdot \cos(\xi_2) \\
&\quad + w_{3,f}\cdot \sin(\xi_3) + b_4,
\end{aligned} \tag{11}$$

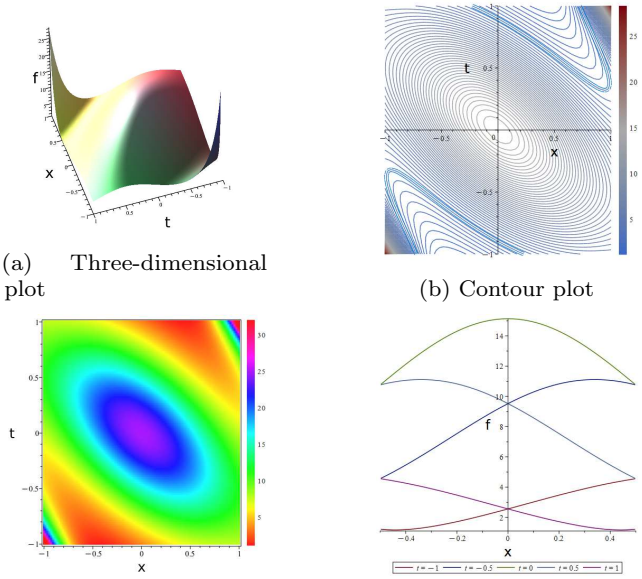
The activation functions are defined as $\Phi_1(\xi_1) = \operatorname{sech}^2(\xi_1)$, $\Phi_2(\xi_2) = \cos(\xi_2)$, and $\Phi_3(\xi_3) = \sin(\xi_3)$.

As shown in Figure 8, with the activation functions set to $\Phi_1(\xi_1) = \operatorname{sech}^2(\xi_1)$, $\Phi_2(\xi_2) = \cos(\xi_2)$, and $\Phi_3(\xi_3) = \sin(\xi_3)$, the probe function for the solution is obtained as follows:

where b_i for $i = 1, 2, 3$, $w_{j,f}$ for $j = 1, 2$, and $w_{k,1}$ for $k = x, t, xt, x^2, t^2$ are real numbers.

Equation (12) is substituted into the CDG equation (1), resulting in a complex algebraic equation. Terms are

$$
\begin{aligned}
f = {} & w_{1,f} \cdot \sinh\left(w_{x,1} \cdot x + w_{t,1} \cdot t + w_{xt,1} \cdot xt + w_{x^2,1} \cdot x^2 + w_{t^2,1} \cdot t^2 + b_1\right) \\
& + w_{2,f} \cdot \cosh\left(w_{x,2} \cdot x + w_{t,2} \cdot t + w_{xt,2} \cdot xt + w_{x^2,2} \cdot x^2 + w_{t^2,2} \cdot t^2 + b_2\right) \\
& + w_{3,f} \cdot e^{\left(w_{x,3} \cdot x + w_{t,3} \cdot t + w_{xt,3} \cdot xt + w_{x^2,3} \cdot x^2 + w_{t^2,3} \cdot t^2 + b_3\right)} + b_4,
\end{aligned} \tag{8}
$$



(a) Three-dimensional plot

(b) Contour plot

(c) Density plot

(d) Curve chart

Fig. 7: Three-dimensional plot, density plot, contour plot and curve chart of the solution to Equation (10)

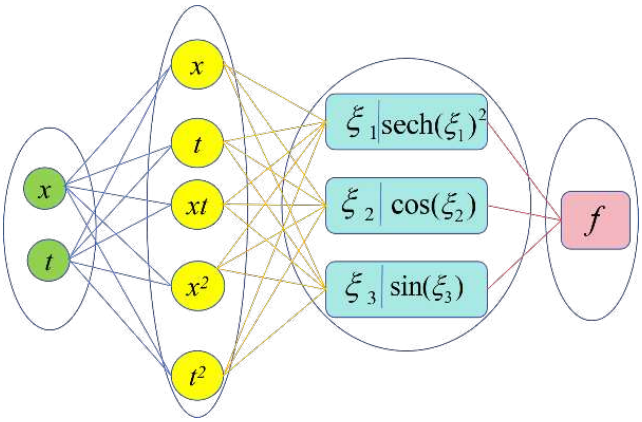


Fig. 8: Single-Hidden Layer Feature Enhancement '2-5-3-1' Neural Network Model

then collated, and the coefficient of each term is equated to zero—a constraint that ensures compliance with the CDG equation. This process yields a system of algebraic equations, whose solution yields the corresponding analytical solution.

Case 1

$$
\begin{cases}
t = t,\ x = x,\ b_4 = b_4,\ w_{1,4} = 0,\ w_{2,4} = 0, \\
w_{3,4} = w_{3,4}, w_{t,1} = w_{t,1},\ w_{t,2} = w_{t,2}, \\
w_{t,3} = -2\hbar w_{t^2,3} - x w_{xt,3}, w_{x,1} = w_{x,1}, \\
w_{x,2} = w_{x,2},\ w_{x,3} = -\hbar w_{xt,3} - 2x w_{x^2,3}, \\
w_{xt,1} = w_{xt,1},\ w_{xt,2} = w_{xt,2},\ w_{xt,3} = w_{xt,3}, \\
w_{t^2,1} = w_{t^2,1},\ w_{t^2,2} = w_{t^2,2}, w_{t^2,3} = w_{t^2,3}, \\
w_{x^2,1} = w_{x^2,1},\ w_{x^2,2} = w_{x^2,2},\ w_{x^2,3} = w_{x^2,3}
\end{cases} \tag{13}
$$

For Case 1, Equation (13) is substituted into Equation (12) and simplified, resulting in the analytical solution of the CDG equation presented in Equation (14):

$$
f = b_4 + w_{3,4} \sin\left(-t^2 w_{t^2,3} - t x w_{xt,3} - x^2 w_{x^2,3} + b_3\right) \tag{14}
$$

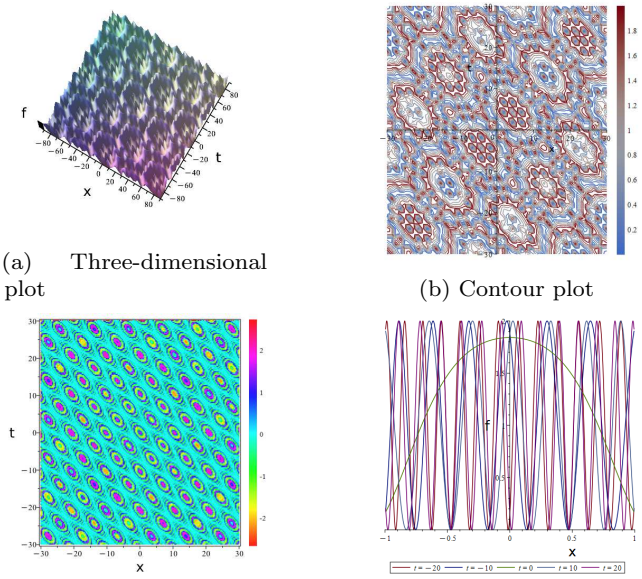
To verify the accuracy of Result (14), the analytical solution corresponding to this result is substituted into the left-hand side of Equation (1). By means of the Maple symbolic computation engine, symbolic simplification confirms that the left-hand side of Equation (1) is equal to zero, thereby validating the reliability, accuracy, and zero-error property of the analytical solution associated with Result (14).

By setting $b_4 = 1$, $w_{3,4} = 1$, $w_{t^2,3} = 2$, $w_{xt,3} = 2$, $w_{x^2,3} = 2$, $b_3 = 1$, the visualization of the solution (Figure 9) is generated:

- Figure 9(a) shows the three-dimensional image for $t \in (-30, 30)$ and $x \in (-30, 30)$;
- Figure 9(b) presents the contour plot of the solution corresponding to Equation (14);
- Figure 9(c) displays the density plot;
- Figure 9(d) depicts the curve plot of u versus x over the domain $(-150, 150)$.

The mathematical expression corresponding to the single-hidden-layer feature-enhanced '2-5-3-1' neural network model in Figure 10 is selected as the probe function:

$$
\begin{aligned}
f = {} & w_{1,f} \cdot \operatorname{sech}^2\left(w_{x,1} \cdot x + w_{t,1} \cdot t + w_{xt,1} \cdot xt + w_{x^2,1} \cdot x^2 + w_{t^2,1} \cdot t^2 + b_1\right) \\
& + w_{2,f} \cdot \cos\left(w_{x,2} \cdot x + w_{t,2} \cdot t + w_{xt,2} \cdot xt + w_{x^2,2} \cdot x^2 + w_{t^2,2} \cdot t^2 + b_2\right) \\
& + w_{3,f} \cdot \sin\left(w_{x,3} \cdot x + w_{t,3} \cdot t + w_{xt,3} \cdot xt + w_{x^2,3} \cdot x^2 + w_{t^2,3} \cdot t^2 + b_3\right) + b_4,
\end{aligned} \tag{12}
$$



(a) Three-dimensional plot

(b) Contour plot

(c) Density plot

(d) Curve chart

Fig. 9: Three-dimensional plot, density plot, contour plot and curve chart of the solution to Equation (14)

$$
\begin{aligned}
\xi_1 = {} & w_{x,1} \cdot x + w_{t,1} \cdot t + w_{xt,1} \cdot xt \\
& + w_{x^2,1} \cdot x^2 + w_{t^2,1} \cdot t^2 + b_1, \\
\xi_2 = {} & w_{x,2} \cdot x + w_{t,2} \cdot t + w_{xt,2} \cdot xt \\
& + w_{x^2,2} \cdot x^2 + w_{t^2,2} \cdot t^2 + b_2, \\
\xi_3 = {} & w_{x,3} \cdot x + w_{t,3} \cdot t + w_{xt,3} \cdot xt \\
& + w_{x^2,3} \cdot x^2 + w_{t^2,3} \cdot t^2 + b_3, \\
f = {} & w_{1,f} \cdot \tanh(\xi_1) + w_{2,f} \cdot \cos(\xi_2) \\
& + w_{3,f} \cdot \sin(\xi_3) + b_4,
\end{aligned} \tag{15}
$$

The activation functions are defined as $\Phi_1(\xi_1) = \tanh(\xi_1)$, $\Phi_2(\xi_2) = \cos(\xi_2)$, and $\Phi_3(\xi_3) = \sin(\xi_3)$.

As shown in Figure 10, with the activation functions set to $\Phi_1(\xi_1) = \tanh(\xi_1)$, $\Phi_2(\xi_2) = \cos(\xi_2)$, and $\Phi_3(\xi_3) = \sin(\xi_3)$, the probe function for the solution is obtained as follows:

where b_i for $i = 1, 2, 3$, $w_{j,f}$ for $j = 1, 2$, and $w_{k,1}$ for $k = x, t, xt, x^2, t^2$ are real numbers.

Equation (16) is substituted into the CDG equation (1), resulting in a complex algebraic equation.Terms are collated, and the coefficient of each term is equated to

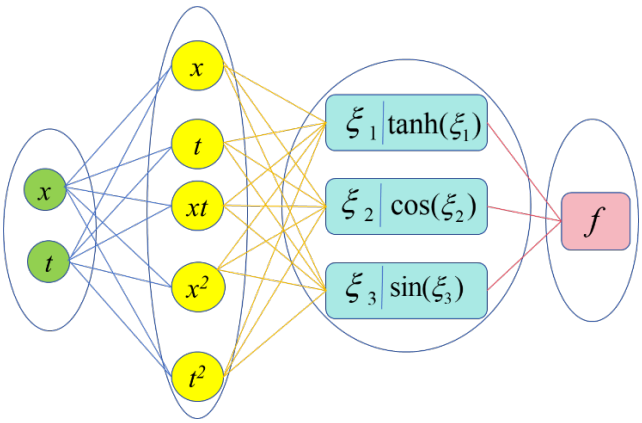


Fig. 10: Single-Hidden Layer Feature Enhancement '2-5-3-1' Neural Network Model

zero—a constraint that ensures compliance with the CDG equation. This process yields a system of algebraic equations, whose solution yields the corresponding analytical solution.

Case 1

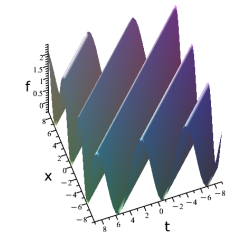
$$
\begin{cases}
b_1 = b_1,\ t = t,\ x = x,\ b_4 = b_4,\ w_{1,4} = w_{1,4}, \\
w_{2,4} = w_{2,4},\ w_{3,4} = w_{3,4},\ w_{t,1} = w_{t,1},\ w_{t,2} = w_{t,2}, \\
w_{t,3} = w_{t,3},\ w_{x,1} = w_{x,1},\ w_{x,2} = w_{x,2},\ w_{x,3} = w_{x,3}, \\
w_{xt,1} = w_{xt,1},\ w_{xt,2} = \dfrac{-(2tw_{t^2,2} + w_{t,2})}{x}, \\
w_{xt,3} = \dfrac{-(2tw_{t^2,3} + w_{t,3})}{x}, w_{t^2,1} = w_{t^2,1},\ w_{t^2,2} = w_{t^2,2}, \\
w_{t^2,3} = w_{t^2,3},\ w_{x^2,1} = w_{x^2,1}, \\
w_{x^2,2} = \dfrac{2t^2 w_{t^2,2} + tw_{t,2} - xw_{xt,2}}{2x^2}, \\
w_{x^2,3} = \dfrac{2t^2 w_{t^2,3} + tw_{t,3} - xw_{xt,3}}{2x^2}
\end{cases} \tag{17}
$$

For Case 1, Equation (17) is substituted into Equation (16) and simplified, resulting in the analytical solution of the CDG equation presented in Equation (18):

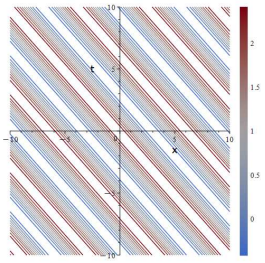
$$
\begin{aligned}
f = {} & b_4 + w_{2,4} \cos\left(\frac{tw_{t,2}}{2} + \frac{xw_{xt,2}}{2} + b_2\right) \\
& + w_{3,4} \sin\left(\frac{tw_{t,3}}{2} + \frac{xw_{xt,3}}{2} + b_3\right)
\end{aligned} \tag{18}
$$

To verify the accuracy of Result (18), the analytical solution associated with this result is substituted into the

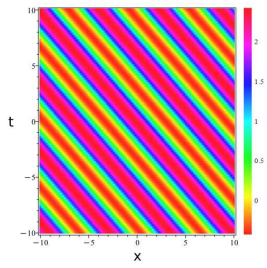
$$
\begin{aligned}
f = {} & w_{1,f} \cdot \tanh\left(w_{x,1} \cdot x + w_{t,1} \cdot t + w_{xt,1} \cdot xt + w_{x^2,1} \cdot x^2 + w_{t^2,1} \cdot t^2 + b_1\right) \\
& + w_{2,f} \cdot \cos\left(w_{x,2} \cdot x + w_{t,2} \cdot t + w_{xt,2} \cdot xt + w_{x^2,2} \cdot x^2 + w_{t^2,2} \cdot t^2 + b_2\right) \\
& + w_{3,f} \cdot \sin\left(w_{x,3} \cdot x + w_{t,3} \cdot t + w_{xt,3} \cdot xt + w_{x^2,3} \cdot x^2 + w_{t^2,3} \cdot t^2 + b_3\right) + b_4,
\end{aligned} \tag{16}
$$



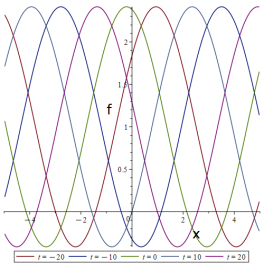
(a) Three-dimensional plot



(b) Contour plot



(c) Density plot



(d) Curve chart

Fig. 11: Three-dimensional plot, density plot, contour plot and curve chart of the solution to Equation (18)

left-hand side of Equation (1). By means of the Maple symbolic computation engine, symbolic simplification confirms that the left-hand side of Equation (1) is equal to zero, thereby validating the reliability, accuracy, and zero-error property of the analytical solution associated with Result (18).

By setting $b_4 = 1$, $w_{2,4} = 1$, $w_{t,2} = 2$, $w_{xt,2} = 2$, $w_{x,3} = 2$, $b_2 = 1$, $w_{3,4} = 1$, $w_{t,3} = 2$, $b_3 = 1$, the visualization of the solution (Figure 11) is generated:

- Figure 11(a) shows the three-dimensional image for $t \in (-30, 30)$ and $x \in (-30, 30)$;
- Figure 11(b) presents the contour plot of the solution corresponding to Equation (18);
- Figure 11(c) displays the density plot;
- Figure 11(d) depicts the curve plot of u versus x over the domain $(-150, 150)$.

The mathematical expression corresponding to the single-hidden-layer feature-enhanced 2-5-3-1 neural network model illustrated in Figure 12 is designated as the probe function.

$$
\begin{aligned}
\xi_1 &= w_{x,1} \cdot x + w_{t,1} \cdot t + w_{xt,1} \cdot xt \\
&\quad + w_{x^2,1} \cdot x^2 + w_{t^2,1} \cdot t^2 + b_1, \\
\xi_2 &= w_{x,2} \cdot x + w_{t,2} \cdot t + w_{xt,2} \cdot xt \\
&\quad + w_{x^2,2} \cdot x^2 + w_{t^2,2} \cdot t^2 + b_2, \\
\xi_3 &= w_{x,3} \cdot x + w_{t,3} \cdot t + w_{xt,3} \cdot xt \\
&\quad + w_{x^2,3} \cdot x^2 + w_{t^2,3} \cdot t^2 + b_3, \\
f &= w_{1,f} \cdot \mathrm{sech}(\xi_1) + w_{2,f} \cdot \tanh(\xi_2) \\
&\quad + w_{3,f} \cdot e^{\xi_3} + b_4,
\end{aligned} \tag{19}
$$

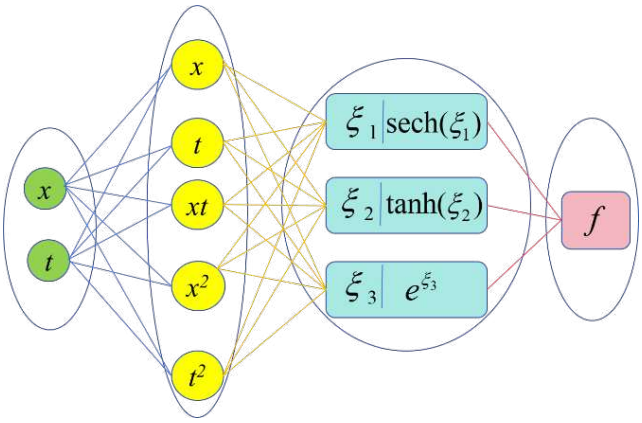


Fig. 12: Single-Hidden Layer Feature Enhancement '2-5-3-1' Neural Network Model

The activation functions are defined as $\Phi_1(\xi_1) = \mathrm{sech}(\xi_1)$, $\Phi_2(\xi_2) = \tanh(\xi_2)$, and $\Phi_3(\xi_3) = e^{\xi_3}$.

As shown in Figure 12, with the activation functions set to $\Phi_1(\xi_1) = \mathrm{sech}(\xi_1)$, $\Phi_2(\xi_2) = \tanh(\xi_2)$, and $\Phi_3(\xi_3) = e^{\xi_3}$, the probe function for the solution is obtained as follows: where b_i for $i = 1, 2, 3$, $w_{j,f}$ for $j = 1, 2, 3$, and $w_{k,1}$ for $k = x, t, xt, x^2, t^2$ are real numbers.

Equation (20) is substituted into the CDG equation (1), leading to a complex algebraic equation. Subsequent collation of terms and equating of the coefficient of each term to zero—constraints that ensure compliance with the CDG equation—yield a system of algebraic equations. Solving this system yields the corresponding analytical solution:

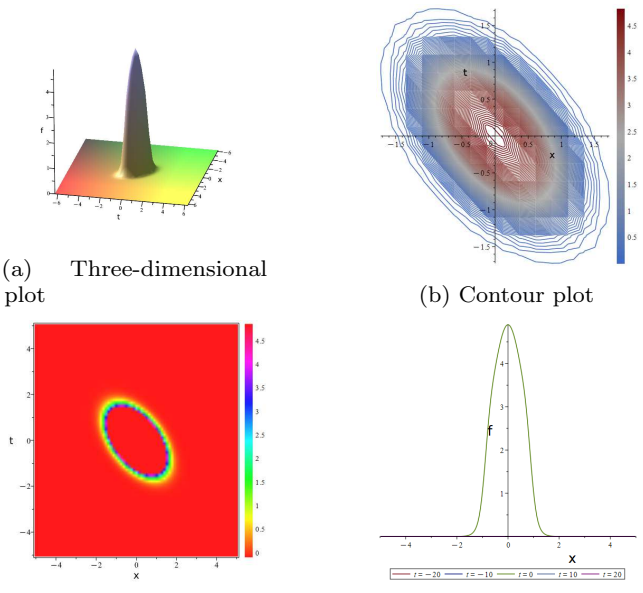
$$
\begin{aligned}
f = {} & w_{1,f} \cdot \operatorname{sech}\left(w_{x,1} \cdot x + w_{t,1} \cdot t + w_{xt,1} \cdot xt + w_{x^2,1} \cdot x^2 + w_{t^2,1} \cdot t^2 + b_1\right) \\
& + w_{2,f} \cdot \tanh\left(w_{x,2} \cdot x + w_{t,2} \cdot t + w_{xt,2} \cdot xt + w_{x^2,2} \cdot x^2 + w_{t^2,2} \cdot t^2 + b_2\right) \\
& + w_{3,f} \cdot e^{\left(w_{x,3} \cdot x + w_{t,3} \cdot t + w_{xt,3} \cdot xt + w_{x^2,3} \cdot x^2 + w_{t^2,3} \cdot t^2 + b_3\right)} + b_4,
\end{aligned} \tag{20}
$$

Case 1

$$
\begin{cases}
t = t,\ x = x,\ b_4 = b_4,\ w_{1,4} = w_{1,4},\ w_{2,4} = w_{2,4}, \\
w_{3,4} = w_{3,4},\ w_{t,1} = -2\hbar w_{t^2,1} - x w_{xt,1}, \\
w_{t,2} = -2\hbar w_{t^2,2} - x w_{xt,2},\ w_{t,3} = -2\hbar w_{t^2,3} - x w_{xt,3}, \\
w_{x,1} = -\hbar w_{xt,1} - 2x w_{x^2,1},\ w_{x,2} = -\hbar w_{xt,2} - 2x w_{x^2,2}, \\
w_{x,3} = -\hbar w_{xt,3} - 2x w_{x^2,3},\ w_{xt,1} = w_{xt,1}, \\
w_{xt,2} = w_{xt,2}, w_{xt,3} = w_{xt,3},\ w_{t^2,1} = w_{t^2,1}, \\
w_{t^2,2} = w_{t^2,2},\ w_{t^2,3} = w_{t^2,3}, \\
w_{x^2,1} = w_{x^2,1},\ w_{x^2,2} = w_{x^2,2},\ w_{x^2,3} = w_{x^2,3}
\end{cases} \tag{21}
$$

For Case 1, Equation (21) is substituted into Equation (20) and simplified, resulting in the analytical solution of the CDG equation presented in Equation (22):

$$
\begin{aligned}
f = {} & b_4 + w_{1,4} \operatorname{sech}^2\left(-t^2 w_{t^2,1} - t x w_{xt,1} - x^2 w_{x^2,1} + b_1\right) \\
& + w_{2,4} \tanh\left(-t^2 w_{t^2,2} - t x w_{xt,2} - x^2 w_{x^2,2} + b_2\right) \\
& + w_{3,4} e^{-t^2 w_{t^2,3} - t x w_{xt,3} - x^2 w_{x^2,3} + b_3}
\end{aligned} \tag{22}
$$



(a) Three-dimensional plot

(b) Contour plot

(c) Density plot

(d) Curve chart

Fig. 13: Three-dimensional plot, density plot, contour plot and curve chart of the solution to Equation (22)

To verify the accuracy of Result (22), the analytical solution associated with this result is substituted into the left-hand side of Equation (1). By means of the Maple symbolic computation engine, symbolic simplification confirms that the left-hand side of Equation (1) is equal to zero, thereby validating the reliability, accuracy, and zero-error property of the analytical solution associated with Result (22).

By setting $b_4 = 1$, $w_{1,4} = 1$, $w_{2,4} = 1$, $w_{3,4} = 1$, $w_{t^2,1} = 2$, $w_{t^2,2} = 2$, $w_{t^2,3} = 2$, $w_{xt,1} = 2$, $w_{xt,2} = 2$, $w_{xt,3} = 2$, $w_{x^2,1} = 2$, $w_{x^2,2} = 2$, $w_{x^2,3} = 2$, $b_3 = 1$, $b_1 = 1$, $b_2 = 1$, the visualization of the solution (Figure 13) is generated:

- Figure 13(a) shows the three-dimensional image for $t \in (-30, 30)$ and $x \in (-30, 30)$;
- Figure 13(b) presents the contour plot of the solution corresponding to Equation (22);
- Figure 13(c) displays the density plot;
- Figure 13(d) depicts the curve plot of u versus x over the domain $(-150, 150)$.

3.2 Dual-Hidden-Layer Feature-Enhanced '2-5-2-2-1' Neural Network Model

The mathematical expression corresponding to the dual-hidden-layer feature-enhanced 2-5-2-2-1 neural network model illustrated in Figure 14 is designated as the probe function:

$$
\begin{aligned}
\xi_1 = {} & w_{x,1} \cdot x + w_{t,1} \cdot t + w_{xt,1} \cdot xt \\
& + w_{x^2,1} \cdot x^2 + w_{t^2,1} \cdot t^2 + b_1, \\
\xi_2 = {} & w_{x,2} \cdot x + w_{t,2} \cdot t + w_{xt,2} \cdot xt \\
& + w_{x^2,2} \cdot x^2 + w_{t^2,2} \cdot t^2 + b_2, \\
\xi_3 = {} & w_{3,1} \xi_1^2 + w_{3,2} e^{\xi_2} + b_3, \\
\xi_4 = {} & w_{4,1} \xi_1^2 + w_{4,2} e^{\xi_2} + b_4, \\
f = {} & b_5 + w_{3,f} \xi_3 + w_{4,f} \tanh(\xi_4),
\end{aligned} \tag{23}
$$

The activation functions are defined as $\Phi_1(\xi_1) = \xi_1^2$, $\Phi_2(\xi_2) = e^{\xi_2}$, $\Phi_3(\xi_3) = \xi_3$, and $\Phi_4(\xi_4) = \tanh(\xi_4)$.

As shown in Figure 14, with the activation functions set to $\Phi_1(\xi_1) = \xi_1^2$, $\Phi_2(\xi_2) = e^{\xi_2}$, $\Phi_3(\xi_3) = \xi_3$, and $\Phi_4(\xi_4) = \tanh(\xi_4)$, the probe function for the solution is obtained as follows: where b_i for $i = 1, 2, 3, 4, 5$, $w_{i,3}$ for $i = 1, 2$, $w_{j,f}$ for $j = 3, 4$, and $w_{k,1}$ for $k = x, t, xt, x^2, t^2$ are real numbers.

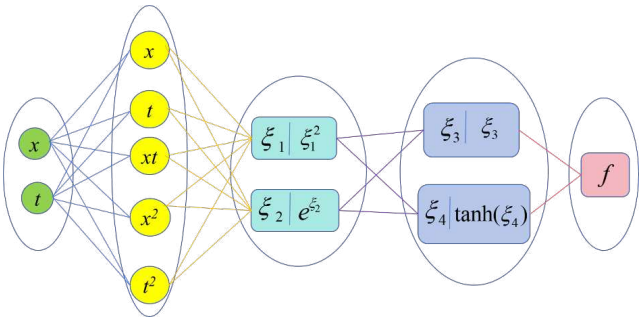


Fig. 14: Dual-Hidden-Layer Feature-Enhanced '2-5-2-2-1' Neural Network Model

Equation (24) is substituted into the CDG equation (1), giving rise to a complex algebraic equation. Through collation of terms and equating of the coefficient of each term to zero—constraints that ensure compliance with the CDG equation—a system of algebraic equations is derived. Solving this system yields the corresponding analytical solution:

Case 1

$$\begin{cases} b_1 = -t^2 w_{t^2,1} + x^2 w_{x^2,1} - t w_{t,1},\ t = t,\ x = x, \\ b_3 = b_3,\ b_5 = b_5,\ w_{1,3} = w_{1,3},\ w_{1,4} = w_{1,4},\ w_{2,3} = w_{2,3}, \\ w_{2,4} = w_{2,4},\ w_{t,1} = w_{t,1},\ w_{t,2} = -2t w_{t^2,2} - x w_{xt,2}, \\ w_{x,1} = -t w_{xt,1} - 2x w_{x^2,1},\ w_{x,2} = -t w_{xt,2} - 2x w_{x^2,2}, \\ w_{xt,1} = w_{xt,1},\ w_{xt,2} = w_{xt,2},\ w_{t^2,1} = w_{t^2,1}, \\ w_{t^2,2} = w_{t^2,2},\ w_{x^2,1} = w_{x^2,1},\ w_{x^2,2} = w_{x^2,2} \end{cases} \tag{25}$$

For Case 1, Equation (25) is substituted into Equation (24) and simplified, resulting in the analytical solution of the CDG equation presented in Equation (26):

$$\begin{aligned} f = {} & e^{\left(-t^2 w_{t^2,2} - t x w_{xt,2} - x^2 w_{x^2,2} + b_2\right)} w_{1,3} w_{1,4} w_{2,3} \\ & + w_{2,4} \tanh\left(w_{2,4} e^{\left(-t^2 w_{t^2,2} - t x w_{xt,2} - x^2 w_{x^2,2} + b_2\right)} + b_4\right) \\ & + b_3 w_{1,4} + b_5 \end{aligned} \tag{26}$$

For Case 1, Equation (25) is substituted into Equation (24) and simplified, resulting in the analytical solution of the CDG equation presented in Equation (26):

To verify the accuracy of Result (26), the analytical solution associated with this result is substituted into the left-hand side of Equation (1). By means of the Maple symbolic computation engine, symbolic simplification confirms that the left-hand side of Equation (1) is equal to zero, thereby validating the reliability, accuracy, and zero-error property of the analytical solution associated with Result (26). Concurrently, this verification further underscores the unique advantages of the dual-hidden-layer architecture: compared with the single-hidden-layer counterpart, the dual-hidden-layer feature-enhanced structure enables more refined hierarchical feature mapping., enabling more accurate capture of the complex coupling mechanisms between fifth-order dispersive terms and strong nonlinear terms in the CDG equation. The extended feature learning space brought by the two hidden layers enhances the model's ability to fit high-dimensional nonlinear relationships, making it more efficient in retrieving analytical solutions with complex structures. This not only confirms the effectiveness of the dual-hidden-layer design in improving solution precision but also further verifies the distinctive value of the FEDSCNN algorithm in breaking through the limitations of traditional analytical methodsand classical neural network approaches that only yield approximate results, as it can directly derive exact analytical expressions for high-order nonlinear wave equations.

By setting $b_4 = 2$, $w_{1,4} = 2$, $w_{2,4} = 2$, $w_{t^2,2} = 1$, $w_{x^2,2} = 1$, $w_{xt,2} = 1$, $w_{2,3} = 2$, $b_3 = 2$, $b_5 = 1$, $b_2 = 1$, the visualization of the solution (Figure 15) is generated:

- Figure 15(a) shows the three-dimensional image for $t \in (-30, 30)$ and $x \in (-30, 30)$;
- Figure 15(b) presents the contour plot of the solution corresponding to Equation (26);
- Figure 15(c) displays the density plot;
- Figure 15(d) depicts the curve plot of u versus x over the domain $(-150, 150)$.

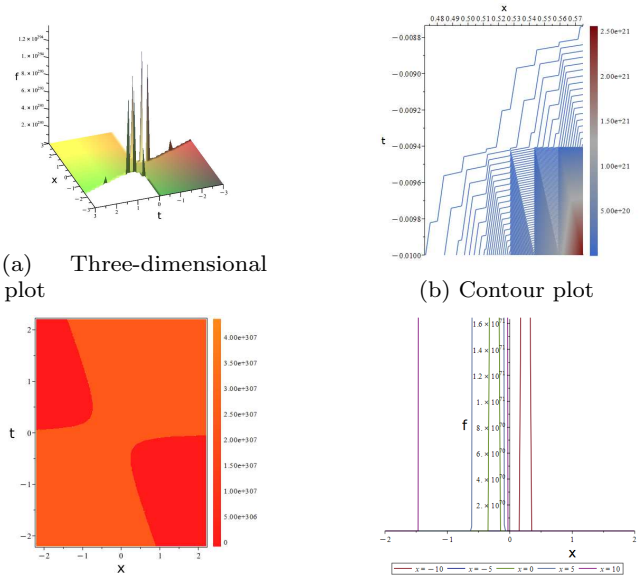
The mathematical expression corresponding to the dual-hidden-layer feature-enhanced "2-5-2-2-1" neural network model illustrated in Figure 16 is chosen as the probe function:

$$\begin{aligned} \xi_1 &= w_{x,1} \cdot x + w_{t,1} \cdot t + w_{xt,1} \cdot xt + w_{x^2,1} \cdot x^2 \\ &\quad + w_{t^2,1} \cdot t^2 + b_1, \\ \xi_2 &= w_{x,2} \cdot x + w_{t,2} \cdot t + w_{xt,2} \cdot xt + w_{x^2,2} \cdot x^2 \\ &\quad + w_{t^2,2} \cdot t^2 + b_2, \\ \xi_3 &= w_{1,3} \xi_1^2 + w_{2,3} e^{\xi_2} + b_3, \\ \xi_4 &= w_{1,3} \xi_1^2 + w_{2,3} e^{\xi_2} + b_4, \\ f &= b_5 + w_{3,f} \mathrm{sech}(\xi_3) + w_{4,f} \tanh(\xi_4), \end{aligned} \tag{27}$$

The activation functions are defined as $\Phi_1(\xi_1) = \xi_1^2$, $\Phi_2(\xi_2) = e^{\xi_2}$, $\Phi_3(\xi_3) = \mathrm{sech}(\xi_3)$, and $\Phi_4(\xi_4) = \tanh(\xi_4)$.

As shown in Figure 16, with the activation functions set to $\Phi_1(\xi_1) = \xi_1^2$, $\Phi_2(\xi_2) = e^{\xi_2}$, $\Phi_3(\xi_3) = \mathrm{sech}(\xi_3)$, and $\Phi_4(\xi_4) = \tanh(\xi_4)$, the probe function for the solution is obtained as follows: where b_i for $i = 1, 2, 3, 4, 5$, $w_{i,3}$ for $i = 1, 2$, $w_{j,f}$ for $j = 3, 4$, and $w_{k,1}$ for $k = x, t, xt, x^2, t^2$ are real numbers.

$$
\begin{aligned}
f = b_5 + w_{3,f} \Big(& w_{3,1} \left(t^2 w_{t^2,1} + t x w_{xt,1} + x^2 w_{x^2,1} + t w_{t,1} + x w_{x,1} + b_1 \right)^2 \\
& + w_{2,3} e^{\left(t^2 w_{t^2,2} + t x w_{xt,2} + x^2 w_{x^2,2} + t w_{t,2} + x w_{x,2} + b_2 \right)} + b_3 \Big) \\
& + w_{4,f} \tanh \Big(w_{1,3} \left(t^2 w_{t^2,1} + t x w_{xt,1} + x^2 w_{x^2,1} + t w_{t,1} + x w_{x,1} + b_1 \right)^2 \\
& + w_{2,3} e^{\left(t^2 w_{t^2,2} + t x w_{xt,2} + x^2 w_{x^2,2} + t w_{t,2} + x w_{x,2} + b_2 \right)} + b_4 \Big),
\end{aligned}
\tag{24}
$$



(a) Three-dimensional plot

(b) Contour plot

(c) Density plot

(d) Curve chart

Fig. 15: Three-dimensional plot, density plot, contour plot and curve chart of the solution to Equation (26)

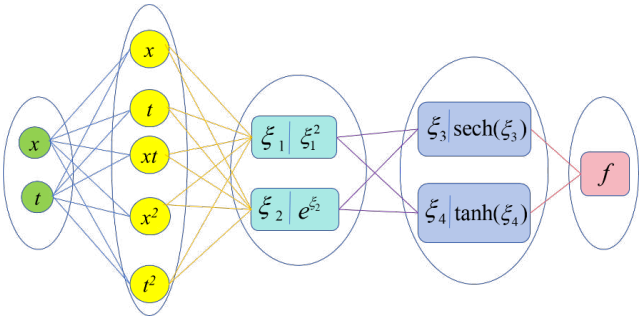


Fig. 16: Dual-Hidden-Layer Feature-Enhanced '2-5-2-2-1' Neural Network Model

Equation (28) is substituted into the CDG equation (1), giving rise to a complex algebraic equation. By collating like terms and equating the coefficient of each term to zero—constraints that ensure compliance with the CDG equation—this process yields a system of algebraic equations. Solving this system yields the corresponding analytical solution.

Case 1

$$
\begin{cases}
b_1 = b_1,\ t = t,\ x = x,\ b_5 = b_5,\ w_{1,3} = 0, \\
w_{1,4} = w_{1,4},\ w_{2,3} = w_{2,3},\ w_{2,4} = 0, \\
w_{t,1} = w_{t,1},\ w_{t,2} = -2t w_{t^2,2} - x w_{xt,2}, \\
w_{x,1} = w_{x,1},\ w_{x,2} = -t w_{xt,2} - 2x w_{x^2,2}, \\
w_{xt,1} = w_{xt,1},\ w_{xt,2} = w_{xt,2},\ w_{t^2,1} = w_{t^2,1}, \\
w_{t^2,2} = w_{t^2,2},\ w_{x^2,1} = w_{x^2,1},\ w_{x^2,2} = w_{x^2,2}
\end{cases}
\tag{29}
$$

For Case 1, Equation (29) is substituted into Equation (28) and simplified, resulting in the analytical solution of the CDG equation presented in Equation (30):

$$
f = w_{1,4} \operatorname{sech} \left(w_{2,3} e^{\left(-t^2 w_{t^2,2} - t x w_{xt,2} - x^2 w_{x^2,2} + b_2 \right)} + b_3 \right) + b_5 \tag{30}
$$

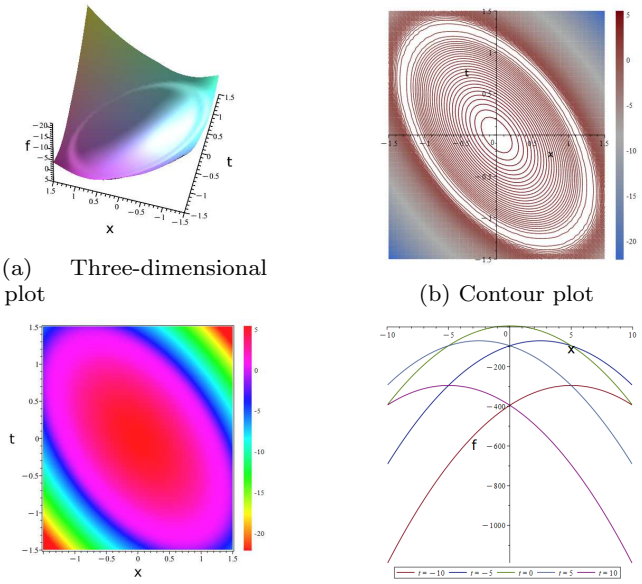
To verify the accuracy of Result (30), the analytical solution associated with this result is substituted into the left-hand side of Equation (1). By means of the Maple symbolic computation engine, symbolic simplification confirms that the left-hand side of Equation (1) is equal to zero, thereby validating the reliability, accuracy, and zero-error property of the analytical solution associated with Result (30).

By setting $b_3 = 2$, $b_5 = 1$, $w_{1,4} = 2$, $w_{t^2,2} = 1$, $w_{x^2,2} = 1$, $w_{xt,2} = 1$, $w_{2,3} = 2$, $b_2 = 1$, the visualization of the solution (Figure 17) is generated:

- Figure 17(a) shows the three-dimensional image for $t \in (-30, 30)$ and $x \in (-30, 30)$;
- Figure 17(b) presents the contour plot of the solution corresponding to Equation (30);
- Figure 17(c) displays the density plot;
- Figure 17(d) depicts the curve plot of u versus x over the domain $(-150, 150)$.

The mathematical expression corresponding to the dual-hidden-layer feature-enhanced 2-5-2-2-1 neural network model illustrated in Figure 18 is designated as the

$$
\begin{aligned}
f = {} & b_5 + w_{3,f}\operatorname{sech}\left(w_{1,3}\left(t^2 w_{t^2,1} + t x w_{xt,1} + x^2 w_{x^2,1} + \hbar w_{t,1} + x w_{x,1} + b_1\right)^2\right. \\
& \left. + w_{2,3} e^{\left(t^2 w_{t^2,2} + t x w_{xt,2} + x^2 w_{x^2,2} + \hbar w_{t,2} + x w_{x,2} + b_2\right)} + b_3\right) \\
& + w_{4,f}\tanh\left(w_{1,3}\left(t^2 w_{t^2,1} + t x w_{xt,1} + x^2 w_{x^2,1} + \hbar w_{t,1} + x w_{x,1} + b_1\right)^2\right. \\
& \left. + w_{2,3} e^{\left(t^2 w_{t^2,2} + t x w_{xt,2} + x^2 w_{x^2,2} + \hbar w_{t,2} + x w_{x,2} + b_2\right)} + b_4\right),
\end{aligned}
\tag{28}
$$



(a) Three-dimensional plot

(b) Contour plot

(c) Density plot

(d) Curve chart

Fig. 17: Three-dimensional plot, density plot, contour plot and curve chart of the solution to Equation (30)

probe function:

$$
\begin{aligned}
\xi_1 &= w_{x,1}\cdot x + w_{t,1}\cdot t + w_{xt,1}\cdot xt + w_{x^2,1}\cdot x^2 \\
&\quad + w_{t^2,1}\cdot t^2 + b_1, \\
\xi_2 &= w_{x,2}\cdot x + w_{t,2}\cdot t + w_{xt,2}\cdot xt + w_{x^2,2}\cdot x^2 \\
&\quad + w_{t^2,2}\cdot t^2 + b_2, \\
\xi_3 &= w_{1,3}\cos(\xi_1) + w_{2,3}\sin(\xi_2) + b_3, \\
\xi_4 &= w_{1,3}\cos(\xi_1) + w_{2,3}\sin(\xi_2) + b_4, \\
f &= b_5 + w_{3,f}\xi_3^2 + w_{4,f}\xi_4^2,
\end{aligned}
\tag{31}
$$

The activation functions are defined as $\Phi_1(\xi_1) = \cos(\xi_1)$, $\Phi_2(\xi_2) = \sin(\xi_2)$, $\Phi_3(\xi_3) = \xi_3^2$, and $\Phi_4(\xi_4) = \xi_4^2$.

As shown in Figure 18, with the activation functions set to $\Phi_1(\xi_1) = \cos(\xi_1)$, $\Phi_2(\xi_2) = \sin(\xi_2)$, $\Phi_3(\xi_3) = \xi_3^2$, and $\Phi_4(\xi_4) = \xi_4^2$, the probe function for the solution is obtained as follows: where b_i for $i = 1, 2, 3, 4, 5$, $w_{i,3}$ for $i = 1, 2$, $w_{j,f}$ for $j = 3, 4$, and $w_{k,1}$ for $k = x, t, xt, x^2, t^2$ are real numbers.

Equation (32) is substituted into the CDG equation (1), giving rise to a complex algebraic equation. By

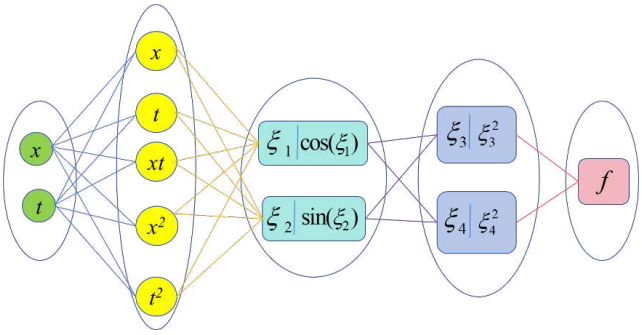


Fig. 18: Dual-Hidden-Layer Feature-Enhanced '2-5-2-2-1' Neural Network Model

collating like terms and equating the coefficient of each term to zero—constraints that ensure compliance with the CDG equation—a system of algebraic equations is derived. Solving this system yields the corresponding analytical solution:

Case 1

$$
\begin{cases}
b_3 = b_3,\ t = t,\ x = x,\ b_5 = b_5,\ w_{1,3} = 0, \\
w_{2,3} = w_{2,3},\ w_{3,f} = w_{3,f},\ w_{4,f} = w_{4,f}, \\
w_{t,2} = -2t w_{t^2,2} - x w_{xt,2},\ w_{t,1} = w_{t,1}, \\
w_{x,2} = -t w_{xt,2} - 2x w_{x^2,2},\ w_{x,1} = w_{x,1}, \\
w_{xt,2} = w_{xt,2},\ w_{xt,1} = w_{xt,1},\ w_{t^2,1} = w_{t^2,1}, \\
w_{t^2,2} = w_{t^2,2},\ w_{x^2,1} = w_{x^2,1},\ w_{x^2,2} = w_{x^2,2}
\end{cases}
\tag{33}
$$

For Case 1, Equation (33) is substituted into Equation (32) and simplified, resulting in the analytical solution of the CDG equation presented in Equation (34):

$$
\begin{aligned}
f = {} & b_5 \\
& + w_{3,f}\left(w_{2,3}\sin\left(-t^2 w_{t^2,2} - t x w_{xt,2} - x^2 w_{x^2,2} + b_2\right) + b_3\right)^2 \\
& + w_{4,f}\left(w_{2,3}\sin\left(-t^2 w_{t^2,2} - t x w_{xt,2} - x^2 w_{x^2,2} + b_2\right) + b_3\right)^2
\end{aligned}
\tag{34}
$$

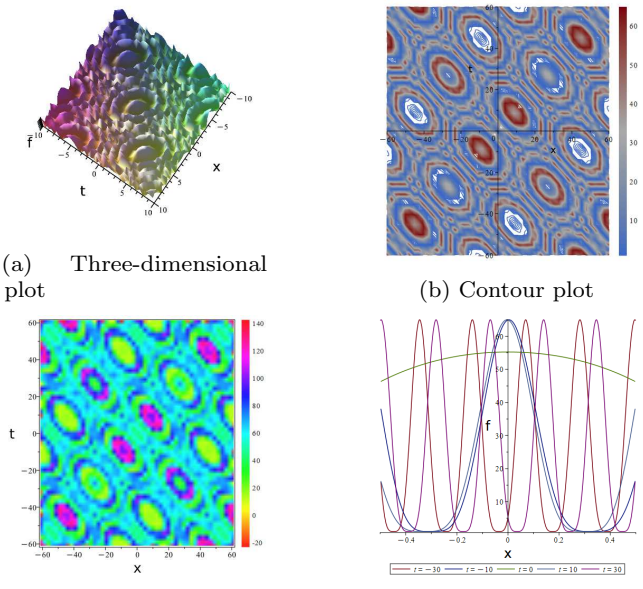
To verify the accuracy of Result (34), the analytical solution associated with this result is substituted into the left-hand side of Equation (1). By means of the Maple symbolic computation engine, symbolic simplification confirms that the left-hand side of Equation (1) is equal to zero, thereby validating the reliability, accuracy, and

$$
\begin{aligned}
f = b_5 + w_{3,f}\,&\left(w_{1,3}\cos\left(t^2 w_{t^2,1} + txw_{xt,1} + x^2 w_{x^2,1} + tw_{t,1} + xw_{x,1} + b_1\right)\right.\\
&\left.+w_{2,3}\sin\left(t^2 w_{t^2,2} + txw_{xt,2} + x^2 w_{x^2,2} + tw_{t,2} + xw_{x,2} + b_2\right) + b_3\right)^2\\
&+ w_{4,f}\left(w_{1,3}\cos\left(t^2 w_{t^2,1} + txw_{xt,1} + x^2 w_{x^2,1} + tw_{t,1} + xw_{x,1} + b_1\right)\right.\\
&\left.+w_{2,3}\sin\left(t^2 w_{t^2,2} + txw_{xt,2} + x^2 w_{x^2,2} + tw_{t,2} + xw_{x,2} + b_2\right) + b_4\right)^2,
\end{aligned}
\tag{32}
$$

zero-error property of the analytical solution associated with Result (34).

By setting $b_3 = 2$, $b_5 = 1$, $w_{3,f} = 2$, $w_{4,f} = 2$, $w_{t^2,2} = 1$, $w_{x^2,2} = 1$, $w_{xt,2} = 1$, $w_{2,3} = 2$, the visualization of the solution (Figure 19) is generated:

- Figure 19(a) shows the three-dimensional image for $t \in (-30, 30)$ and $x \in (-30, 30)$;
- Figure 19(b) presents the contour plot of the solution corresponding to Equation (34);
- Figure 19(c) displays the density plot;
- Figure 19(d) depicts the curve plot of u versus x over the domain $(-150, 150)$.



(a) Three-dimensional plot

(b) Contour plot

(c) Density plot

(d) Curve chart

Fig. 19: Three-dimensional plot, density plot, contour plot and curve chart of the solution to Equation (34)

4 Conclusion

This study addresses the challenge of obtaining exact solutions for the fifth-order dispersive CDG equation by proposing the FEDSCNN algorithm. The work provides an efficient novel approach for the analytical solution of high-order nonlinear wave equations. The principal research conclusions are as follows:

Algorithm Construction and Innovative Breakthroughs.The FEDSCNN algorithm successfully integrates the adaptive feature extraction capability of neural networks, the rigour of symbolic computation, and the advantages of feature enhancement. Two network architectures tailored for the CDG equation are constructed: a single-hidden-layer '2-5-3-1' architecture and a dual-hidden-layer '2-5-2-2-1' architecture. Polynomial feature enhancement intensifies the interaction between higher-order dispersive terms and strong nonlinear interaction terms, while embedded physical constraints ensure solution consistency. This proposed methodology dispenses with the prerequisite for pre-defined solution paradigms and mitigates reliance on discrete transforms, thereby effectively overcoming the inherent limitations of traditional analytical methodologies—constraints that entail restricted applicability scope, heightened computational complexity, and inadequate feature representation capabilities in contemporary neural network architectures.

Significant Advances in Exact Solution Acquisition.Through the adoption of the FEDSCNN algorithm, a diverse spectrum of exact solutions to the CDG equation has been successfully retrieved, encompassing soliton solutions and periodic solutions constructed via sine, cosine, hyperbolic tangent, and hyperbolic secant functions. All analytical solutions underwent rigorous validation utilizing the Maple symbolic computation engine, which corroborated that substituting these solutions into the CDG equation yields a zero value on the left-hand side. This not only yields error-free solutions but also corroborates the accuracy and reliability of the FEDSCNN algorithm. To vividly characterize the spatiotemporal propagation behaviors of diverse solutions, three-dimensional plots, density plots, contour maps, and curve diagrams were generated. These visualizations thereby provide intuitive theoretical support for understanding wave propagation mechanisms under conditions of strong dispersion and intense nonlinear coupling.

Distinct Performance Advantages of the FEDSCNN Algorithm.In comparison with conventional analytical techniques (e.g., the inverse scattering transform method and Hirota's bilinear method), the FEDSCNN algorithm exhibits independence from the strict integrability of

equations. This inherent characteristic enables it to circumvent intricate variable transformations and the issue of "expression bloat". In contrast to classical neural network-based approaches, its integrated feature enhancement mechanism facilitates the enhanced capture of fifth-order derivative terms, it also achieves faster convergence rates and directly generates analytical expressions rather than approximate solutions. Endowed with inherent generality, the algorithm is not only applicable to the CDG equation but also provides a reusable framework for solving analogous fifth-order KdV-type high-order nonlinear wave equations, such as the Sawada-Kotera equation.

Interdisciplinary Value and Application Prospects.This study fosters the in-depth integration of neural networks and symbolic computation in the field of mathematical physics, paving a novel pathway for the intelligent solution of high-order nonlinear wave equations. The exact solutions obtained for the CDG equation establish a solid theoretical foundation for investigating relevant physical phenomena.These solutions encompass the investigation of physical phenomena such as the propagation of shallow water waves in fluid systems and the evolution of plasma acoustic waves. Furthermore, the design principles inherent to the FEDSCNN algorithm provide valuable insights for the analytical solution of more complex partial differential equations (e.g., fractional-order and variable-coefficient equations), thereby endowing the research with substantial theoretical and practical significance.

Future research may further extend the application scope of the FEDSCNN algorithm to higher-dimensional scenarios, including 3+1-dimensional cases, variable-coefficient modifications, and fractional-order extensions of the CDG equation. Optimizing the feature enhancement module and network architecture is expected to improve the algorithm's adaptability to more complex nonlinear systems. Additionally, exploring its potential in solving inverse problems—such as coefficient identification and order recognition—deserves in-depth investigation.

Author contributions

Jianglong Shen: Conceptualization, methodology, validation, writing–original draft preparation, writing–review and editing, supervision, project administration, funding acquisition; Xia Li: Conceptualization, methodology, validation, writing–review and editing, supervision, project administration, funding acquisition. All authors have read and approved the final version of the manuscript for publication.

Data Availability Statements

No Data associated in the manuscript.

Conflict of Interest:

The authors declare that they have no conflicts of interest.

References

1. Ablowitz, M.J., Clarkson, P.A.: Solitons, nonlinear evolution equations and inverse scattering. Book (1991). DOI 10.1017/CBO9780511623998
2. Sulem, P., Sulem, C.: Nonlinear optics with phase-modulated pulses. Phys. Rev. A **33**, 1532–1539 (1986)
3. Wazwaz, A.M.: Partial Differential Equations and Solitary Waves Theory. Springer, New York (2012). DOI 10.1007/978-3-642-00251-9
4. Aiyer, R.N., Fuchssteiner, B., Oevel, W.: Solitons and discrete eigenfunctions of the recursion operator of nonlinear evolution equations: I. the caudrey-dodd-gibbon-sawada-kotera equations. J. Phys. A: Math. Gen. **19**, 3755–3770 (1986)
5. Coudery, P.J., Dodd, R.K., Gibbon, J.D.: A new hierarchy of korteweg-de vries equations. Proc. R. Soc. A **351**, 407–422 (1976). DOI 10.1098/rspa.1976.0149
6. Rani, A., Ashraf, M., Ahmad, J., Ul-Hassan, Q.M.: Soliton solutions of the caudrey–dodd–gibbon equation using three expansion methods and applications. Opt. Quant. Electron. **54**, 158 (2022). DOI 10.1007/s11082-022-03547-5
7. Qin, M., Wang, Y., Yuen, M.: Optimal system, symmetry reductions and exact solutions of the (2+1)-dimensional seventh-order caudrey–dodd–gibbon–kp equation. Symmetry **16**, 403 (2024). DOI 10.3390/sym16040403
8. Zakharov, V.E., Shabat, A.B.: Exact theory of two-dimensional self-focusing and one-dimensional self-modulation of waves in nonlinear media. J. Exp. Theor. Phys. **34**, 62–69 (1970)
9. Hirota, R.: Exact solution of the korteweg-de vries equation for multiple colliding solitons. Phys. Rev. Lett. **27**, 1192–1194 (1971). DOI 10.1103/PhysRevLett.27.1192
10. Wu, P.X., Yang, Q., He, J.H.: Solitary waves of the variant boussinesq-burgers equation in a fractal-dimensional space. Fractals **30**, 2250056 (2022). DOI 10.1142/S0218348X22500566
11. Olver, P.J.: Applications of Lie Groups to Differential Equations. Springer, New York (1993). DOI 10.1007/978-1-4612-4350-2
12. Rafique, M.N.: Exact solutions of fifth-order sawada-kotera and caudrey-dodd-gibbon equations using unified method. Results Phys. **48**, 110623 (2025). DOI 10.1016/j.rinp.2025.110623
13. Yue, H.T., Deng, Y., Nahmod, A.R.: Invariance of gibbs measures for 2d higher-order nonlinear schrödinger equations and 3d third-order nonlinear wave equations. Ann. Math. **199**, 1051–1128 (2024). DOI 10.4007/annals.2024.199.3.5
14. Koepf, W.: Computer Algebra: An Algorithm-Oriented Introduction. Springer, Cham (2021). DOI 10.1007/978-3-030-78017-3

15. Arif, F., Zaman, F.D., Mahomed, F.M., et al.: Lie symmetry analysis, exact solutions, and conservation laws of a nonlinear convection-diffusion wave equation. Results Eng. **22**, 101852 (2025). DOI 10.1016/j.rineng.2025.101852
16. Raissi, M., Perdikaris, P., Karniadakis, G.E.: Physics-informed neural networks: A deep learning framework for solving forward and inverse problems involving nonlinear partial differential equations. J. Comput. Phys. **378**, 686–707 (2019). DOI 10.1016/j.jcp.2018.10.045
17. Sirignano, J., Spiliopoulos, K.: Dgm: A deep learning algorithm for solving partial differential equations. J. Comput. Phys. **375**, 1339–1364 (2018). DOI 10.1016/j.jcp.2018.08.029
18. Zhu, Z., Peng, X., Zhang, Y., et al.: Solving nonlinear partial differential equations using deep learning with operator-informed regularization. J. Comput. Phys. **418**, 109524 (2020). DOI 10.1073/pnas.1718942115
19. Song, J.H., Cao, W.B., Zhang, W.W.: Fenn: Feature-enhanced neural network for solving partial differential equations involving fluid mechanics. J. Comput. Phys. **542**, 114370 (2025). DOI 10.1016/j.jcp.2025.114370
20. Xie, X.R., Zhang, R.F.: Neural network-based symbolic calculation approach for solving the korteweg–de vries equation. Chaos Solitons Fractals **194**, 116232 (2025). DOI 10.1016/j.chaos.2025.116232
21. Luo, K., Zhao, J., Wang, Y., et al.: Physics-informed neural networks for pde problems: a comprehensive review. Artif. Intell. Rev. **58**, 323 (2025). DOI 10.1007/s10462-025-11322-7
22. Dong, S.C., Li, Z.W.: Local extreme learning machines and domain decomposition for solving linear and nonlinear partial differential equations. Comput. Methods Appl. Mech. Eng. **387**, 114129 (2021). DOI 10.1016/j.cma.2021.114129
23. Tang, S.P., Feng, X.L., Wu, W., Xu, H.: Physics-informed neural networks combined with polynomial interpolation to solve nonlinear partial differential equations. Comput. Math. Appl. **132**, 48–62 (2023). DOI 10.1016/j.camwa.2022.12.008
24. Li, X., Chen, J., Zhang, S.: Fractional physics-informed neural networks with adaptive activation and fractional gradient enhancement. Chaos Solitons Fractals **182**, 114897 (2024). DOI 10.1016/j.chaos.2024.114897
25. Chen, Y., Liu, S., Zhang, H.: Enhanced physics-informed neural networks for higher-order kdv-type equations: Forward and inverse problems. Nonlinear Dyn. **119**, 3217–3238 (2025). DOI 10.1007/s11071-025-09218-7
26. Zeng, S.J., Zhang, Z., Zou, Q.S.: Physics-informed neural networks for solving the heat conduction equation with variable coefficients. Comput. Math. Appl. **84**, 220–232 (2022). DOI 10.1016/j.camwa.2021.08.014
27. Zhang, W., Suo, W., Song, J., et al.: Physics-informed neural networks (pinns) as intelligent computing technique for solving partial differential equations: Limitation and future prospects. Sci. China Phys. Mech. Astron. **69**, 214602 (2026). DOI 10.1007/s11433-024-2665-5
28. Khater, M.M.A., Alfalqi, S.H.: Analytical solutions of the caudrey–dodd–gibbon equation using khater ii and variational iteration methods. Sci. Rep. **14**, 27946 (2024). DOI 10.1038/s41598-024-75969-y
29. Ma, H.C., Wang, Y.X., Deng, A.P.: Soliton molecules and some novel mixed solutions for the extended caudrey-dodd-gibbon equation. J. Geom. Phys. **168**, 104309 (2021). DOI 10.1016/j.geomphys.2021.104309
30. Gai, L.T., et al.: Lump wave solutions, lump-stripe soliton inelastic collision phenomena and rogue-type wave solutions for a generalized breaking soliton system in (3+1)-dimensions. Wave Motion **124**, 103243 (2024). DOI 10.1016/j.wavemoti.2023.103243
31. Shen, J.L., Zhang, R.F., Huang, J.W., Liang, J.B.: Neural network-based symbolic computation algorithm for solving (2+1)-dimensional yu-toda-sasa-fukuyama equation. Mathematics **13**, 3006 (2025). DOI 10.3390/math13183006
32. Wu, X.S., Liu, J.G.: Solving the variable coefficient nonlinear partial differential equations based on the bilinear residual network method. Nonlinear Dyn. **112**, 8329–8340 (2024). DOI 10.1007/s11071-024-09472-4
33. Murad, M.A.S., Alshammari, F.S., Salih, M.S., et al.: Optical soliton structures in the nonlinear conformable schrödinger equation with quadratic–cubic nonlinearity. Nonlinear Dyn. **113**, 32669–32687 (2025). DOI 10.1007/s11071-025-11775-z
34. Hussain, E., Tedjani, A.H., Farooq, K., Beenish: Modeling and exploration of localized wave phenomena in optical fibers using the generalized kundu–eckhaus equation for femtosecond pulse transmission. Axioms **14**, 513 (2025). DOI 10.3390/axioms14070513
35. Li, X., Shen, J.L., Liang, J.B., Gao, Y.: Bilinear feature-enhanced symbolic computation neural network method for solving the (1+1)-dimensional caudrey–dodd–gibbon equation. AIMS Math. **11**, 3193–3218 (2026). DOI 10.3934/math.2026128